Chemical visualization of individual chondrocytes in articular cartilage by attenuated-total-reflection Fourier Transform Infrared Microimaging

Jianhua Yin and Yang Xia*

Department of Physics and Center for Biomedical Research, Oakland University, Rochester, MI 48309, USA
**xia@oakland.edu*

Abstract: Fourier transform infrared imaging (FTIRI) and the attenuated total reflection Fourier transform infrared microimaging (ATR-FTIRM) were used to study the chemical and structural distributions of cellular components surrounding individual chondrocytes in canine humeral cartilage, at 6.25μm pixel resolution in FTIRI and 1.56μm pixel resolution in ATR-FTIRM. The chemical and structural distributions of the cellular components in chondrocytes and tissue can be successfully imaged in high resolution ATR-FTIRM. One can also study the territorial matrix of fine collagen fibrils surrounding the individual chondrocytes by the polarization experiments using the absorption ratio of amide I to amide II bands.

OCIS codes: (110.3080) Infrared imaging; (120.6200) Spectrometers and spectroscopic instrumentation; (170.1530) Cell analysis; (170.3880) Medical and biological imaging; (170.3890) Medical optics instrumentation; (300.6340) Spectroscopy, infrared.

References and links

1. T. Hardingham, S. Tew, and A. Murdoch, "Tissue engineering: chondrocytes and cartilage," Arthritis Res. **4**(Suppl 3), S63–S68 (2002).
2. R. A. Stockwell, "Chondrocytes," J. Clin. Pathol. Suppl. (R Coll Pathol) **12**, 7–13 (1978).
3. K. Tavakol, R. G. Miller, D. P. Bazett-Jones, W. S. Hwang, L. E. McGann, and N. S. Schachar, "Ultrastructural changes of articular cartilage chondrocytes associated with freeze-thawing," J. Orthop. Res. **11**(1), 1–9 (1993).
4. M. Brittberg, A. Lindahl, A. Nilsson, C. Ohlsson, O. Isaksson, and L. Peterson, "Treatment of deep cartilage defects in the knee with autologous chondrocyte transplantation," N. Engl. J. Med. **331**(14), 889–895 (1994).
5. A. C. Hall, "Volume-sensitive taurine transport in bovine articular chondrocytes," J. Physiol. **484**(Pt 3), 755–766 (1995).
6. S. Hashimoto, R. L. Ochs, F. Rosen, J. Quach, G. McCabe, J. Solan, J. E. Seegmiller, R. Terkeltaub, and M. Lotz, "Chondrocyte-derived apoptotic bodies and calcification of articular cartilage," Proc. Natl. Acad. Sci. U.S.A. **95**(6), 3094–3099 (1998).
7. E. Kolettas, H. I. Muir, J. C. Barrett, and T. E. Hardingham, "Chondrocyte phenotype and cell survival are regulated by culture conditions and by specific cytokines through the expression of Sox-9 transcription factor," Rheumatology (Oxford) **40**(10), 1146–1156 (2001).
8. C. C. Scott, A. Luttge, and K. A. Athanasiou, "Development and validation of vertical scanning interferometry as a novel method for acquiring chondrocyte geometry," J. Biomed. Mater. Res. A **72A**(1), 83–90 (2005).
9. S. J. Curran, R. Chen, J. M. Curran, and J. A. Hunt, "Expansion of human chondrocytes in an intermittent stirred flow bioreactor, using modified biodegradable microspheres," Tissue Eng. **11**(9-10), 1312–1322 (2005).
10. H. Yamaoka, H. Asato, T. Ogasawara, S. Nishizawa, T. Takahashi, T. Nakatsuka, I. Koshima, K. Nakamura, H. Kawaguchi, U. I. Chung, T. Takato, and K. Hoshi, "Cartilage tissue engineering using human auricular chondrocytes embedded in different hydrogel materials," J. Biomed. Mater. Res. A **78A**(1), 1–11 (2006).
11. J. A. Ryan, E. A. Eisner, G. DuRaine, Z. You, and A. Hari Reddi, "Mechanical compression of articular cartilage induces chondrocyte proliferation and inhibits proteoglycan synthesis by activation of the ERK pathway: implications for tissue engineering and regenerative medicine," J. Tissue Eng. Regen. Med. **3**(2), 107–116 (2009).
12. I. K. Y. Lo, P. Sciore, M. Chung, S. Liang, R. B. Boorman, G. M. Thornton, J. B. Rattner, and K. Muldrew, "Local anesthetics induce chondrocyte death in bovine articular cartilage disks in a dose- and duration-dependent manner," Arthroscopy J. Arthroscopic. Rel. Surg. **25**(7), 707–715 (2009).
13. J.-H. Yin and Y. Xia, "Macromolecular concentrations in bovine nasal cartilage by Fourier transform infrared imaging and principal component regression," Appl. Spectrosc. **64**(11), 1199–1208 (2010).

#140139 - $15.00 USD Received 22 Dec 2010; revised 16 Mar 2011; accepted 17 Mar 2011; published 18 Mar 2011

14. Y. Xia, N. Ramakrishnan, and A. Bidthanapally, "The depth-dependent anisotropy of articular cartilage by Fourier-transform infrared imaging (FTIRI)," Osteoarthritis Cartilage **15**(7), 780–788 (2007).
15. N. Ramakrishnan, Y. Xia, and A. Bidthanapally, "Polarized IR microscopic imaging of articular cartilage," Phys. Med. Biol. **52**(15), 4601–4614 (2007).
16. Y. Xia, H. Alhadlaq, N. Ramakrishnan, A. Bidthanapally, F. Badar, and M. Lu, "Molecular and morphological adaptations in compressed articular cartilage by polarized light microscopy and Fourier-transform infrared imaging," J. Struct. Biol. **164**(1), 88–95 (2008).
17. N. P. Camacho, P. West, P. A. Torzilli, and R. Mendelsohn, "FTIR microscopic imaging of collagen and proteoglycan in bovine cartilage," Biopolymers **62**(1), 1–8 (2001).
18. P. A. West, M. P. G. Bostrom, P. A. Torzilli, and N. P. Camacho, "Fourier transform infrared spectral analysis of degenerative cartilage: an infrared fiber optic probe and imaging study," Appl. Spectrosc. **58**(4), 376–381 (2004).
19. X. Bi, X. Yang, M. P. Bostrom, and N. P. Camacho, "Fourier transform infrared imaging spectroscopy investigations in the pathogenesis and repair of cartilage," Biochim. Biophys. Acta **1758**(7), 934–941 (2006).
20. H. J. Gulley-Stahl, S. B. Bledsoe, A. P. Evan, and A. J. Sommer, "The advantages of an attenuated total internal reflection infrared microspectroscopic imaging approach for kidney biopsy analysis," Appl. Spectrosc. **64**(1), 15–22 (2010).
21. S. G. Kazarian and K. L. A. Chan, "Micro- and macro-attenuated total reflection Fourier transform infrared spectroscopic imaging," Appl. Spectrosc. **64**(5), 135–152 (2010).
22. J. Lee, E. Gazi, J. Dwyer, M. D. Brown, N. W. Clarke, J. M. Nicholson, and P. Gardner, "Optical artefacts in transflection mode FTIR microspectroscopic images of single cells on a biological support: the effect of back-scattering into collection optics," Analyst (Lond.) **132**(8), 750–755 (2007).
23. R. A. Dluhy, "Infrared spectroscopy of biophysical monomolecular films at interfaces: theory and applications, " Appl. Spectrosc. Rev. **35**(4), 315–351 (2000).
24. J. Dunham, D. R. Shackleton, M. E. Billingham, L. Bitensky, J. Chayen, and I. H. Muir, "A reappraisal of the structure of normal canine articular cartilage," J. Anat. **157**, 89–99 (1988).
25. S. Z. Wang, Y. P. Huang, Q. Wang, Y. P. Zheng, and Y. H. He, "Assessment of depth and degeneration dependences of articular cartilage refractive index using optical coherence tomography in vitro," Connect. Tissue Res. **51**(1), 36–47 (2010).
26. C. V. Koulis, J. A. Reffner, and A. M. Bibby, "Comparison of transmission and internal reflection infrared spectra of cocaine," J. Forensic Sci. **46**(4), 822–829 (2001).
27. N. Jamin, P. Dumas, J. Moncuit, W. H. Fridman, J. L. Teillaud, G. L. Carr, and G. P. Williams, "Highly resolved chemical imaging of living cells by using synchrotron infrared microspectrometry," Proc. Natl. Acad. Sci. U.S.A. **95**(9), 4837–4840 (1998).
28. Y. Xia, J. B. Moody, H. Alhadlaq, and J. N. Hu, "Imaging the physical and morphological properties of a multi-zone young articular cartilage at microscopic resolution," J. Magn. Reson. Imaging **17**(3), 365–374 (2003).
29. H. A. Alhadlaq, Y. Xia, F. M. Hansen, C. M. Les, and G. Lust, "Morphological changes in articular cartilage due to static compression: polarized light microscopy study," Connect. Tissue Res. **48**(2), 76–84 (2007).

1. Introduction

Articular cartilage, a compliant load-bearing surface covering the ends of bones, comprises an extracellular matrix (ECM) embedded with living cells, the chondrocytes. The ECM of articular cartilage principally consists of water, type II collagen and aggregated proteoglycan molecules. The physical properties of articular cartilage depend on the structure and organization of the collagen network and the concentration of proteoglycans in the tissue [1], which are maintained by the functional activity of chondrocytes [2]. As a result of trauma or degenerative joint diseases, cartilage is frequently damaged and difficult to be repaired due its avascular nature and no recruitment of healthy cells to the site of damage [1]. Although the structure, geometry and function of chondrocytes have been studied extensively by many techniques such as microscopies, biological and biomechanical methods [2–12], the molecular/chemical components and their distribution inside/around the chondrocytes are difficult to study.

Fourier transform infrared Imaging (FTIRI), which uses the imaging approach to study spectroscopically chemical concentrations and distributions, has become a powerful tool in biomedical research. For example, it is possible to spatially resolve various chemical signatures with a fine spatial pixel size (e.g., 6.25μm) and a spectral resolution (e.g. 1-16cm^{-1}) in cartilage [13]. FTIRI can also be very effective in the study of the orientation of the chemical bonds (e.g., amide I bond, which is the C = O in a molecular dipole) in cartilage [14,15], the changes in the collagen orientation due to external loading [16], and the molecular concentrations in cartilage [13,17–19]. The main limitation of FTIRI is its spatial resolution, on the order of 5-10 microns due to its optical properties.

#140139 - $15.00 USD Received 22 Dec 2010; revised 16 Mar 2011; accepted 17 Mar 2011; published 18 Mar 2011

The use of an attenuated total reflection (ATR) accessory in FTIRI could break this optical limitation [20]. With a germanium crystal, which has a high refractive index of 4.0 in the ATR accessory, the ATR FTIR microimaging (ATR-FTIRM) can improve the pixel resolution by a factor of four (from 6.25μm to 1.56μm in a commercial PerkinElmer FTIRI system). The purpose of this study is to determine if individual chondrocytes can be optically visualized and chemically measured by ATR-FTIRM to provide insights into the fine structure and molecular distribution of chondrocytes in articular cartilage.

2. Experimental

A number of unstained 6μm-thick sections of canine humeral articular cartilage were obtained in a cryostat and mounted on low-E glass slides (Kevley Technologies, Chesterland, OH) for ATR-FTIRM and FTIRI experiments on a PerkinElmer Spotlight 300 infrared imaging system (Wellesley, MA). This system is equipped with a FTIR spectrometer for spectrum collection, a liquid N_2 cooled 16-element mercuric cadmium telluride focal plane array detector for the rapid acquisition of FTIR images, and a motorized stage on which the specimen slides can be mounted. An internal coaxial LED illumination with variable intensity is available to produce visible images, which enables the identification of the region of interest (ROI) for infrared imaging. The FTIRI data were collected at 6.25μm pixel resolution and 16cm^{-1} spectral resolution, with 2 scans per pixel over a spectral range of 4000-744cm^{-1}.

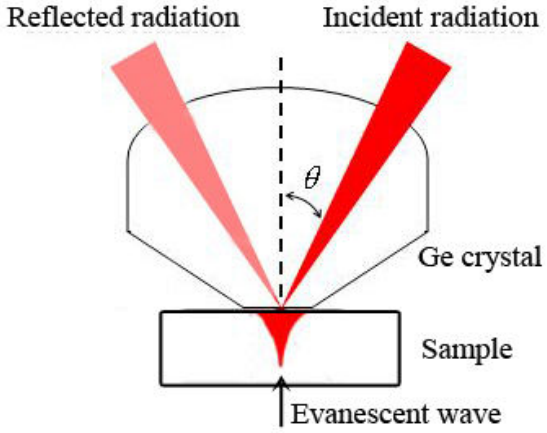

Fig. 1. Graphical Representation of ATR.

The ATR-FTIRM experiments were performed on the same infrared imaging system with the addition of an ATR accessory. By removing the lower cassegrain, a germanium crystal mounted on a rotate-able arm [20] can be lowered to make a delicate contact with the specimen on the glass slide, as shown in Fig. 1. When the total reflection happens in the germanium crystal, an evanescent wave is orthogonally projected on to the sample. A part of energy of the evanescent wave is absorbed by the sample so that the IR beam energy is attenuated as being reflected to the detector. This accessory improves the pixel resolution in the imaging system by a factor of four, from 6.25μm to 1.56μm. The ATR images were processed using an ATR image background that contains a set of spectra from crystal without the specimen. The ROI of 200μm × 200μm was imaged in the spectral ranging of 4000-744cm^{-1}, with the same spectral resolution of 16cm^{-1} and 2 scans per pixel. A wire grid IR polarizer, inserted between the sample and detector, was used as an analyzer in the imaging experiments to polarize the light between 0° and 90°. Since the penetration depth of the IR beam in the specimen increases with the wavelength of the radiation [21], the effective path length of the ATR-FTIR spectra varies with the wavelength of the radiation. The ATR correction was therefore performed for all ATR-FTIR spectra based on the assumption that

#140139 - $15.00 USD Received 22 Dec 2010; revised 16 Mar 2011; accepted 17 Mar 2011; published 18 Mar 2011

the contact between the ATR crystal and the tissue section was ideal. In addition to the infrared imaging experiments, the ROI in the ATR-FTIRM were imaged using a Leica microscope with a 40 × objective (0.20μm/pixel) to obtain a high quality visible image.

3. Results and discussion

3.1. Chemical and structural analysis

Figure 2a shows the visible image of one cartilage section, with its articular surface at the top of the image. The total absorbance images from FTIRI and ATR-FTIRM were shown in Fig. 2b and 2c, respectively. It is clear that the ATR image could resolve much more detail of the tissue section. There are several features of these two infrared images. First, some cells in the ATR image exhibited weaker absorption, especially at the cellular centers, than the *same* cells in the FTIR image, which were highlighted as conglomerations. This feature can be attributed to light scattering at these cell areas in transflection FTIR imaging [20,22], which is different from the application of total reflection principle in ATR imaging. At the same time, the penetration depth in ATR imaging would reduce to no more than a few microns [21,23]. At an angle of incidence approximately 30° at the sample and when the radiation wavelength is 10μm (1000cm^{-1}), the penetration depth to the tissue would be about 1.18μm, from a critical angle of 21.6° due to the refractive index of the dry cartilage section reported at 1.475 [24]. Consequently, the penetration of the infrared irradiation in ATR experiments would be less than the section thickness (6μm) and effectively avoid the transflection and the effect of tissue thickness on cell imaging [22]. Another feature of the ATR image is the high-intensity regions (the red region in Fig. 2c) at the superficial zone (SZ) of the tissue, which is mostly caused by the higher refractive index at SZ than that at the transitional zone (TZ) [25], resulting in the increases in penetration depth and subsequent absorbance [21,23]. An identical ATR imaging experiment was carried out using a section of bovine nasal cartilage, which did not show this high intensity feature at the tissue boundary (data not shown).

Figure 2d shows two spectra, obtained at the same location around a cell in the tissue section, one from the FTIR image and the other from the ATR-FTIR microimage. Unlike the ATR spectrum, a monotonically sloping baseline is visible in the FTIR spectrum, denoting that the spectral artifact in FTIRI can be attributed to the infrared scattering phenomenon [20]. Another difference between the FTIR spectrum and the ATR-FTIR spectrum is the red shift of the amide I, amide II and 3296 cm^{-1} bands of the ATR spectrum relative to those of FTIR spectrum (e.g., 1656 to 1640 cm^{-1}, 1552 to 1544 cm^{-1}, 3328 to 3296 cm^{-1}), which is due to the changes in the refractive index of tissue with irradiation wavelength [26]. At the edge of high contrasts (e.g., tissue surface and air), the use of ATR can reduce some spectral artifacts (spectra not shown), which show as spectral distortion and highlighted region, resulting from the specular reflection and the anomalous dispersion [20].

Figure 3 shows the FTIR images and the ATR-FTIR images at the same area of interest in the tissue section in details, including the chemi-maps of amide II (representing the protein in the cellular imaging [27]) and sugar bands (1100-1000cm^{-1}, representing nucleic acid, carbohydrates and glycogen etc.). Both amide II and sugar images in Fig. 3c show that the distribution of solid components is mainly on the circumference of the cell, as well as at the center of the cell. In comparison, the chemi-maps of amide II and sugar from the FTIR image (Fig. 3a) contain essentially no structural features inside any individual cell, again reflecting the averaging nature in low-resolution imaging. The stronger total absorbance for the cells is due to the artifact caused by the cell scattering effect in transflection FTIRI [20,22].

#140139 - $15.00 USD Received 22 Dec 2010; revised 16 Mar 2011; accepted 17 Mar 2011; published 18 Mar 2011

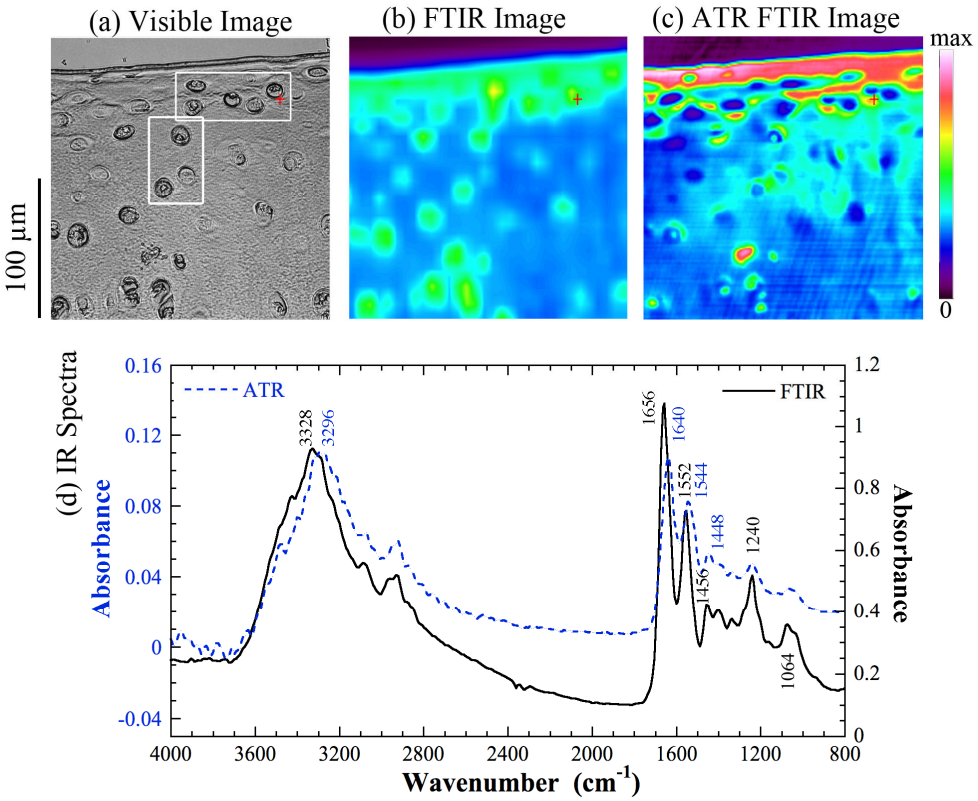

Fig. 2. (a) The visible image, (b) the FTIR image, (c) the ATR-FTIR image of the same region on a cartilage section. The articular surface is near the top of the images. (d) The IR spectra extracted from the FTIR image and ATR-FTIR image at same location with red cross in the tissue section, expressing as solid curve and dashed curve, respectively. The rectangle regions of interest in the transitional zone and superficial zone in (a) would be closely examined in Fig. 3 and Fig. 4.

At several locations in one cell, the spectra were extracted and shown in Fig. 3b and 3d. These marks were selected from the interterritorial regions (6, 7, 14, 15), near/on the cell walls (1, 11), at the center of the cells (4, 12), and in-between the cell wall and cell center (2, 3, 5). The spectra from the FTIR image have more consistent features among all pixels of 11~15, as drawn in Fig. 3b. This consistency is likely caused by the averaging effect of a large pixel (6.25µm) and the scattering effect in transflection imaging [20,22]. The ATR-FTIR spectra in Fig. 3d, by comparison, show many differences in the spectral features at different cellular locations. The spectra at the locations of 2, 3, and 5 were very similar; the same were for the spectra from the locations of 6 and 7. The similarity and differences illustrate that the ATR imaging has not only the spatial but also the spectral resolution to differentiate the molecular and chemical structures among the cell wall, pericellular matrix, and interterritorial regions. It is interesting to note that the spectral absorption was the weakest at the #2 location, which is in between the cell wall and the cell center, probably indicating the less solid component inside the cell on the dried section. Also shown in Fig. 3d, amide I band (indicated by the left dash line) tends to blue-shift followed with shoulder peaks, which denotes that the principal component of protein reduces rapidly and the other component contents (e.g., nucleic acid, glycogen, etc) increase relatively. The spectral analyses for several cells show the similar result.

#140139 - $15.00 USD Received 22 Dec 2010; revised 16 Mar 2011; accepted 17 Mar 2011; published 18 Mar 2011

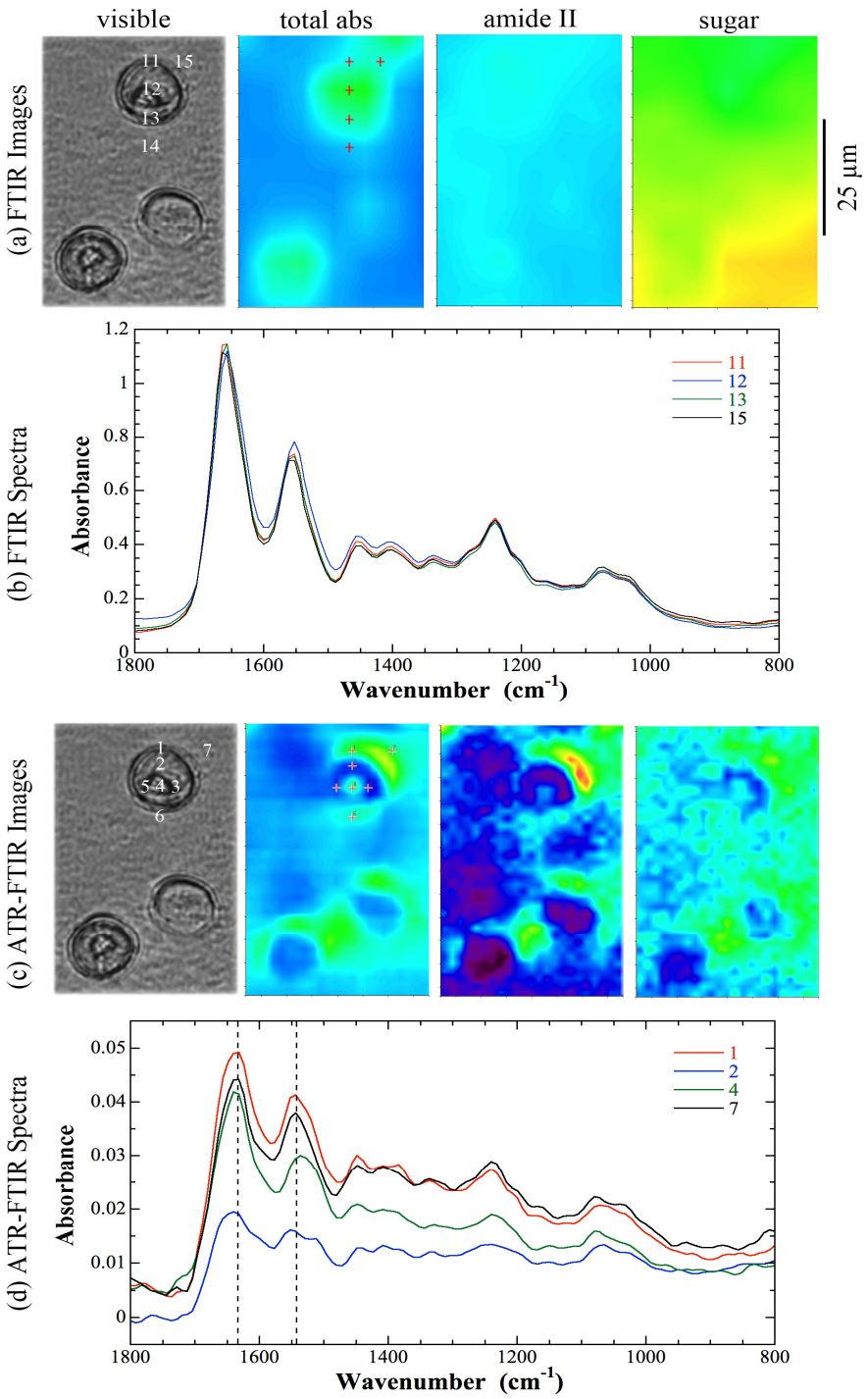

Fig. 3. The detailed region in the transitional zone of the tissue from both the FTIRI (a) and ATR-FTIRM (c) experiments. Four images are shown from each experiment: the visible image, the total absorption image (4000-744cm^{-1}), the amide II image (1580-1500cm^{-1}), and the sugar image (1100-1000cm^{-1}). The infrared spectra from the marked spatial locations are shown in (b) and (d). Two dash lines in (d) indicate the approximate locations of amide I and amide II bands.

#140139 - $15.00 USD Received 22 Dec 2010; revised 16 Mar 2011; accepted 17 Mar 2011; published 18 Mar 2011

3.2. Anisotropy analysis

Infrared dichroism is often used in spectroscopy and imaging to determine the structural orientation and anisotropy of the specimen, since the absorbance of the irradiation beam is unique for parallel polarization and perpendicular polarization. Two orientational relationships are important in the polarization study of articular cartilage. First, when the tissue section is placed in the x-y plane and irradiated by an incident light at an angle to the x-axis in the x-z plane, the reflected light would also be in the x-z plane. At the 0° and 90° polarizations, the infrared vibration would be in the x-z plane and the x-y plane, respectively, both perpendicular to the light path. Second, the amide I and amide II vibrations are approximately perpendicular and parallel to the long axis of collagen fibril in cartilage [14,16]. In this project, the same tissue section was imaged by the ATR-FTIRM twice with the insertion of an infrared polarizer, which sets the irradiation polarization to be parallel (0°) and perpendicular (90°), respectively. Since the absorbance of irradiation at parallel polarization is obviously more than the absorbance of irradiation at perpendicular polarization in this report, which makes it challenging to compare the absorbance of vibrational bands directly. This difficulty is resolved by comparing, instead, the ratios of amide I to amide II when the irradiation polarization is parallel and perpendicular. Figure 4 shows the absorption ratio images of amide I to amide II bands, under the parallel irradiation and the perpendicular irradiation.

It's clear that the absorption ratios of SZ at the parallel polarization (Fig. 4a) are stronger than those at the perpendicular polarization (Fig. 4b). This is because that when a fibril is in parallel with the articular surface (such as in SZ), an irradiation beam polarized parallelly (i.e., at 0°) will induce more amide I absorption than amide II, which results in a stronger ratio of amide I to amide II, as illustrated by the bigger ratio values in SZ in Fig. 4a. In contrast, a perpendicularly polarized irradiation (90°) will reduce the absorption of amide I but increase the absorption of amide II, hence reducing the absorption ratio in SZ in Fig. 4b. This result confirms that the collagen fiber alignment in SZ is indeed in parallel with the cartilage surface. Furthermore, the deeper portion of TZ starts to contain more perpendicular fibers, which causes the lower portion of the image in Fig. 4b to have the increasingly bigger ratios of amide I to amide II with the perpendicular polarization.

Two regions (the horizontal box for the tissue in SZ, and the vertical box for the tissue in TZ) in each absorption ratio image are enlarged in Fig. 4 to show the details of the anisotropy around and at the cells. The elliptical shapes were the locations of the cells as determined on the visible image (Fig. 2a). By comparing the same region of tissue under two mutually orthogonal polarizations, one can notice in TZ at 90° polarization (Fig. 4d) that the absorption ratios at the vertical edges of the three cells are always higher than those at the same locations at the horizontal edges of the cells. The same regions at 0° polarization show a reversed trend - the ratio at the vertical edges weakens while the horizontal edges of the cells become superior. Similar opposing features can also be identified around the cells in SZ (Fig. 4c).

The absorption ratios around the cells were analyzed quantitatively and statistically by grouping the values pixel by pixel around the cells in those images. For each cell analyzed, the absorption ratios in a rectangular region of three pixels by two pixels were extracted and averaged at the horizontal edges of the cells (both the top and bottom edges). At the vertical edges of each cell (both the left and right edges), the absorption ratios in a rectangular region of two pixels by three pixels were extracted and averaged. The regions were chosen on and just outside the lines of the elliptical shapes in Fig. 4c and 4d. The two plots in Fig. 4 show the statistical results from one cell in SZ (the top left cell) and one cell in TZ (the bottom left cell).

#140139 - $15.00 USD Received 22 Dec 2010; revised 16 Mar 2011; accepted 17 Mar 2011; published 18 Mar 2011

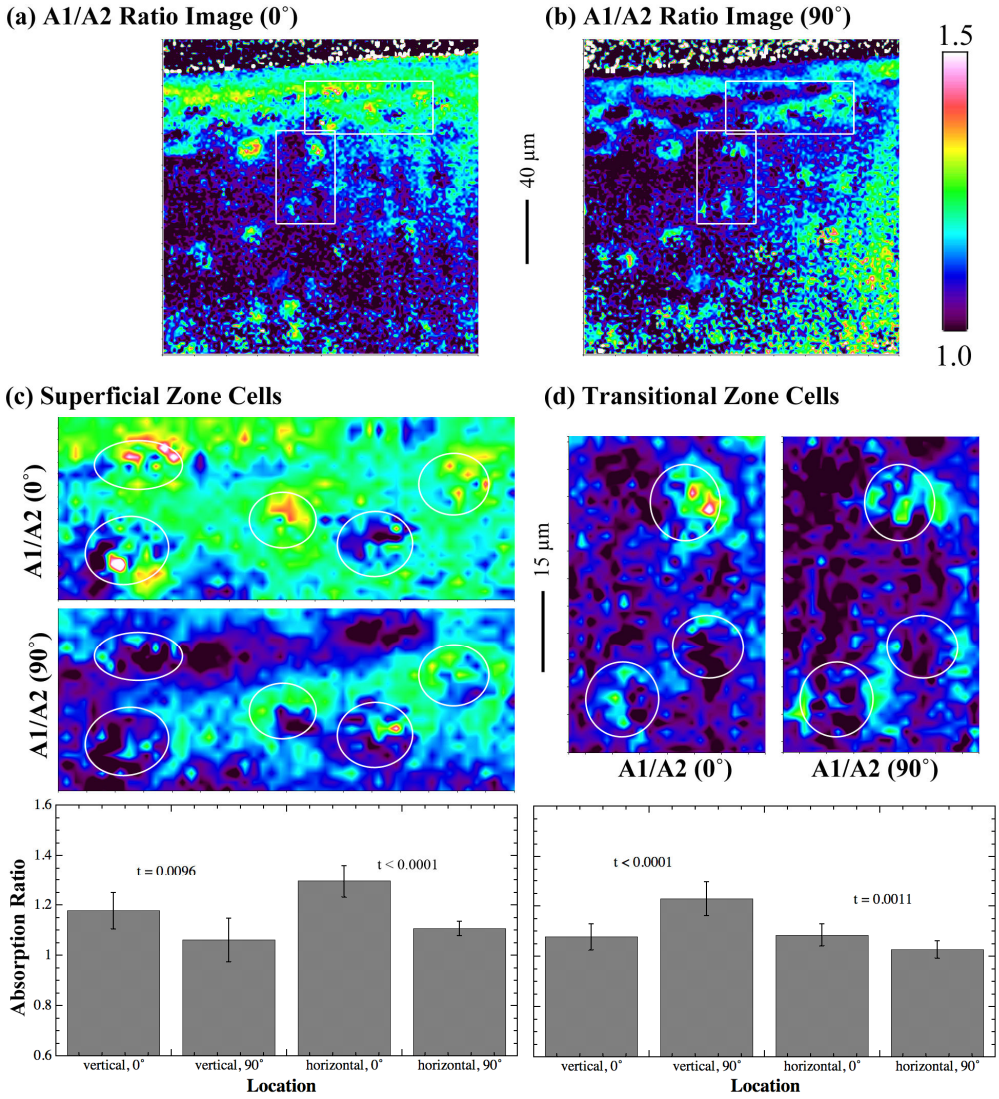

Fig. 4. The anisotropic images of amide I to amide II absorption ratios obtained by using analyzer at (a) parallel polarization (0°) and (b) perpendicular polarization (90°), respectively. The same rectangular regions as shown in Fig. 2a were also shown. (c) and (d) show the detailed regions of the anisotropic images of absorption ratios at the superficial zone and the transitional zone. The elliptical shapes mark the locations and orientations of the individual cells, identified from the high-resolution visible image (Fig. 2a). The two plots under Fig. 4c and 4d show the statistical analysis around the cell walls at the vertical and horizontal edges at 0° and 90° polarizations, respectively.

For the absorption ratios in TZ (the plot under Fig. 4d), both sets of comparisons have statistical significance and also show the opposite trends, i.e., the vertical edge absorption ratio at 0° is lower than that at 90°, while the horizontal edge absorption ratio at 0° is higher than that at 90°. These features confirm the 'cocoon' shaped territorial matrix surrounding each chondrocyte, which is known in literature by a number of high resolution studies [28,29]. For the absorption ratios in SZ (the plot under Fig. 4c), with the horizontal comparison is statistically significant and also consistent with the TZ results, i.e., the visualization of the territorial matrix around each cell. The vertical comparison in SZ, although also significant,

#140139 - $15.00 USD Received 22 Dec 2010; revised 16 Mar 2011; accepted 17 Mar 2011; published 18 Mar 2011

does not fit the matrix structure. One possible cause of errors in the vertical edge could be due to the fact that the chondrocytes are usually smaller and flatter in SZ than in TZ, hence it is difficult to identify the vertical edges of the horizontally oriented elliptical shape in cells at SZ.

4. Conclusion

This preliminary project is the first cellular study to image the individual chondrocytes in articular cartilage by a high-resolution ATR-FTIRM, which effectively overcomes some limitations in FTIRI. Based on the principle of the total reflection, the ATR-FTIRM can examine the individual chondrocytes, not just spatially but also chemically. This ability to study the cells at 1-2μm resolution can provide much enhanced information about the fine structure and chemical component distributions in chondrocytes. The protein mostly distributes around the cells. The polarization comparison of amide I to amide II ratios confirms the collagen fiber orientation surrounding the individual cells. In addition, this high resolution approach can significantly improve the principal component identification and visualization of the individual chondrocytes in ECM. Additional investigations are ongoing in our lab.

Acknowledgments

Yang Xia is grateful to the National Institutes of Health for the R01 grants (AR 045172, AR 052353). The authors are indebted to Drs. C. Les and H. Sabbah (Henry Ford Hospital, Detroit) for providing the canine specimens, and Ms. Carol Searight (Dept. of Physics, Oakland University) for the editorial comments on the manuscript.

#140139 - $15.00 USD Received 22 Dec 2010; revised 16 Mar 2011; accepted 17 Mar 2011; published 18 Mar 2011